Mimicking extracellular matrix-mediated mechano-activation by antibodies to control signaling of the adhesion G protein-coupled receptor GPR126/ADGRG6

Jakob Mitgau*[1], Julius Franke*[1], Camilla Schinner[2], Gabriele Stephan[3], Sandra Berndt[1], Dimitris G. Placantonakis[3,4], Hermann Kalwa[5], Volker Spindler[2], Caroline Wilde[1] and Ines Liebscher[#1]

[1]Rudolf Schönheimer Institute for Biochemistry, Molecular Biochemistry, University of Leipzig, Leipzig, Germany

[2]Department of Biomedicine, University of Basel, Basel, Switzerland

[3]Department of Neurosurgery, NYU Grossman School of Medicine, New York, NY 10016, USA

[4]Kimmel Center for Stem Cell Biology, Laura and Isaac Perlmutter Cancer Center, NYU Grossman School of Medicine, New York, NY 10016, USA

[5]Rudolf-Boehm-Institute for Pharmacology and Toxicology, University of Leipzig, Leipzig, Germany

*contributed equally

[#]Corresponding author: Ines Liebscher

E-mail: ines.liebscher@medizin.uni-leipzig.de.

Running title: Antibodies mimicking mechano-activation of GPR126/ADGRG6

Abstract

The adhesion G protein-coupled receptor (aGPCR) GPR126/ADGRG6 plays an important role in several physiological functions, such as myelination, peripheral nerve repair and osteoblast differentiation, which renders the receptor an attractive pharmacological target. GPR126 is a mechano-sensor that incorporates signals from the extracellular matrix (ECM) through binding to its N-terminal ligands collagen IV and laminin 211. Since ECM components are not suitable therapeutics alternate compounds with more favorable characteristics would be desirable that can mimic the physiologic activation pattern. Antibodies could present an apt alternative as they can specifically target the N-terminus of the receptor, reach multiple tissue compartments and have been shown to modulate GPCR activity levels.

In this study, we use a monoclonal antibody targeting an N-terminal HA-epitope to induce receptor signaling, which can be enhanced through the addition of secondary antibodies. Using single cell atomic force microscopy (AFM) in combination with a fluorescent cAMP sensor, we show that antibody-mediated activation is achieved through combined pushing and pulling forces, while collagen IV and laminin 211 only mediate GPR126 activation through pushing or pulling, respectively. Thus, the antibody-mediated approach can reliably mimic the activation induced by both endogenous ligands. Our findings show that antibody-mediated activation for GPR126 is feasible and can be used for precise targeting of this receptor, thereby establishing it as a pharmaceutical target.

Introduction

The adhesion G protein coupled receptor (aGPCR) GPR126/ADGRG6 plays an essential role in several important physiologic and pathogenic processes, including myelination (***Mogha et al., 2013; Monk et al., 2009; Monk et al., 2011; Ravenscroft et al., 2015***), peripheral nerve injury and repair (***Mogha et al., 2016***), the development of the peripheral nervous system (PNS) (***Ravenscroft et al., 2015***), and the differentiation of osteoblasts (***Sun et al., 2020***) and adipocytes (***Suchý et al., 2020***). Further, an association of *GPR126* variants with the development of scoliosis was found in humans and mice (***Karner et al., 2015; Kou et al., 2013; Kou et al., 2018; Liu et al., 2018; Man et al., 2019; Qin et al., 2017; Takeda et al., 2019; Xu et al., 2015; Xu***, E. ***et al., 2019b; Xu***, E. ***et al., 2019a; Xu***, L. ***et al., 2019***). Thus, pharmacological targeting of this receptor is of high interest. The physiological implications are mainly attributed to the modulation of cAMP levels by the receptor, which is achieved through the receptor's coupling to G_s protein (***Mogha et al., 2013***). The N-terminus of GPR126 includes 5 structurally different domains (***Leon et al., 2020***) among them the autoproteolysis-inducing (GAIN) domain (***Arac et al., 2012***) at which the receptor is autoproteolytically cleaved at the conserved HLT motif within the GPCR proteolytic site (GPS) (***Lin et al., 2004; Moriguchi et al., 2004***). Further, GPR126 undergoes furin-mediated cleavage within the SEA domain (***Leon et al., 2020***).

Like other aGPCRs GPR126 harbors an endogenous tethered agonistic sequence located distal of the GPS cleavage motif, termed the *Stachel* sequence (***Liebscher et al., 2014)***. Synthetic peptides derived from this integral agonist can be used as agonists on the receptor (***Demberg et al., 2017; Liebscher et al., 2014***). Further, small molecule agonists have been identified (***Bradley et al., 2019; Diamantopoulou et al., 2019***), but similar to the agonistic peptides, they lack specificity for the receptor (***Demberg et al., 2017***). Additional activation can be achieved through the receptor's ligands, which each bind to specific parts of the N-terminus. Collagen IV (***Paavola et al., 2014***) and Prion protein PrP^C (***Küffer et al., 2016***) directly activate the receptor to increase cAMP levels. Laminin 211 (***Petersen et al., 2015***), however, has a more complex mode of action. Under static conditions laminin 211 inhibits cAMP formation, but it enhances cAMP levels after addition of mechanical forces. Besides their different modes of action, both laminin 211 and collagen IV are components of the basal lamina, where they play an important role in GPR126-mediated myelination. This indicates that these extracellular matrix (ECM) ligands modulate the activity of GPR126 in distinct and specific manners.

ECM proteins do not display the characteristics of a classic receptor agonist as they are long-lived, stable molecules with essentially no diffusivity. Thus, it is unclear how the interaction

between the aGPCR and the ECM can be interpreted as a signal to modulate receptor activity levels. Mechanical forces generated by the interaction of the aGPCR with the ECM are theorized to represent this signal (***Liebscher et al., 2014; Stoveken et al., 2015***). This theory is supported by the observed second messenger generation upon shaking and vibration of cells overexpressing GPR126 (***Petersen et al., 2015***) and another aGPCR GPR114 (***Wilde et al., 2016***). However, the force input needed to activate these aGPCRs has not been defined. Major obstacles in studying ligand-induced mechano-activation of aGPCRs are the unfavorable physicochemical characteristics of ECM interaction partners, such as poor solubility, as well as the low specificity of the interaction between the ECM and the receptor. An additional difficulty stems from the non-physiological properties of experimental models of mechano-activation, such as vibration and shaking. Such models not only fail to quantify the magnitude of forces needed for receptor activation, but are also not amenable to pharmacological screens. Being able to mimic the ECM-mediated activation patterns on GPR126 will significantly increase our understanding of these functional interactions and structure-function relations in mechano-transduction.

In this study, we use an antibody recognizing an N-terminal HA epitope on GPR126 as an agonist, whose activity-inducing effects is modulated through incubation with a secondary antibody. We employ this setup to investigate the roles of the N-terminus and cleavage sites of GPR126 for mechano-activation. Using single cell atomic force microscopy (AFM) in combination with a fluorescent cAMP sensor, we determine in real time the type and strength of mechanical input needed to activate GPR126 through the antibody-based approach, and through the natural GPR126 ligands collagen IV and laminin 211. We show that the antibody mediates mechanical forces that are also employed by the ligands, which allows to mimic the physiological activation patterns of these complex proteins using a specific, easy to modify molecule. Our findings have mechanistic implications for the activation mechanisms of GPR126 and likely other aGPCRs and might set the stage for pharmaceutical targeting of the receptor.

Results

An antibody targeting the N-terminal HA epitope can activate GPR126

Since GPR126 can be activated through interaction with its ligands and mechanical stimuli, it can be assumed that the N-terminus plays a decisive role in mediating these signals. However, our understanding of these dynamic processes is limited. In order to mimic mechanical forces that could activate GPR126, we established an antibody-based approach, since antibodies show high-affinity and highly specific interactions with their antigens. Because there is no antibody available targeting GPR126 directly at the N-terminus, we used the hemagglutinin (HA) epitope for our experimental setup and inserted it right after the predicted signal peptide of wildtype (WT) GPR126 (Fig. 1A). Increasing concentrations of a commercially available anti-HA antibody significantly elevated cAMP levels in COS-7 cells transfected with the HA-tagged GPR126 (Fig. 1B), but not in the empty vector transfected control cells.

Adding increasing concentrations of a secondary antibody to a stable concentration of 1 µg/ml of the anti-HA antibody yielded an even stronger activation of the receptor (Fig. 1C/D). In order to elucidate whether the observed activation is a consequence of receptor cross-linking through the antibodies or due to the additional weight being attached to the receptor N-terminus, we added anti-HA antibody-conjugated paramagnetic Dynabeads®, which are decisively larger in size than antibodies, to cells transfected with HA-tagged GPR126 (Fig. 1E). We observed a significant increase in cAMP levels (Fig. 1F), which was comparable with anti HA-mediated activation alone (Fig. 1B) but lower than the combination of primary and secondary antibody (Fig. 1E), indicating that simply adding weight is not the sole key to GPR126 activation. In line with this observation, exposure to a 700 Gs magnetic field placed below the cell layer cannot further enhance conjugated Dynabead-mediated activation (Suppl. Fig. S1A). In a control experiment with an anti-FLAG antibody targeting the C-terminal epitope of GPR126 no change in cAMP levels was observed (Supp. Fig. S1B).

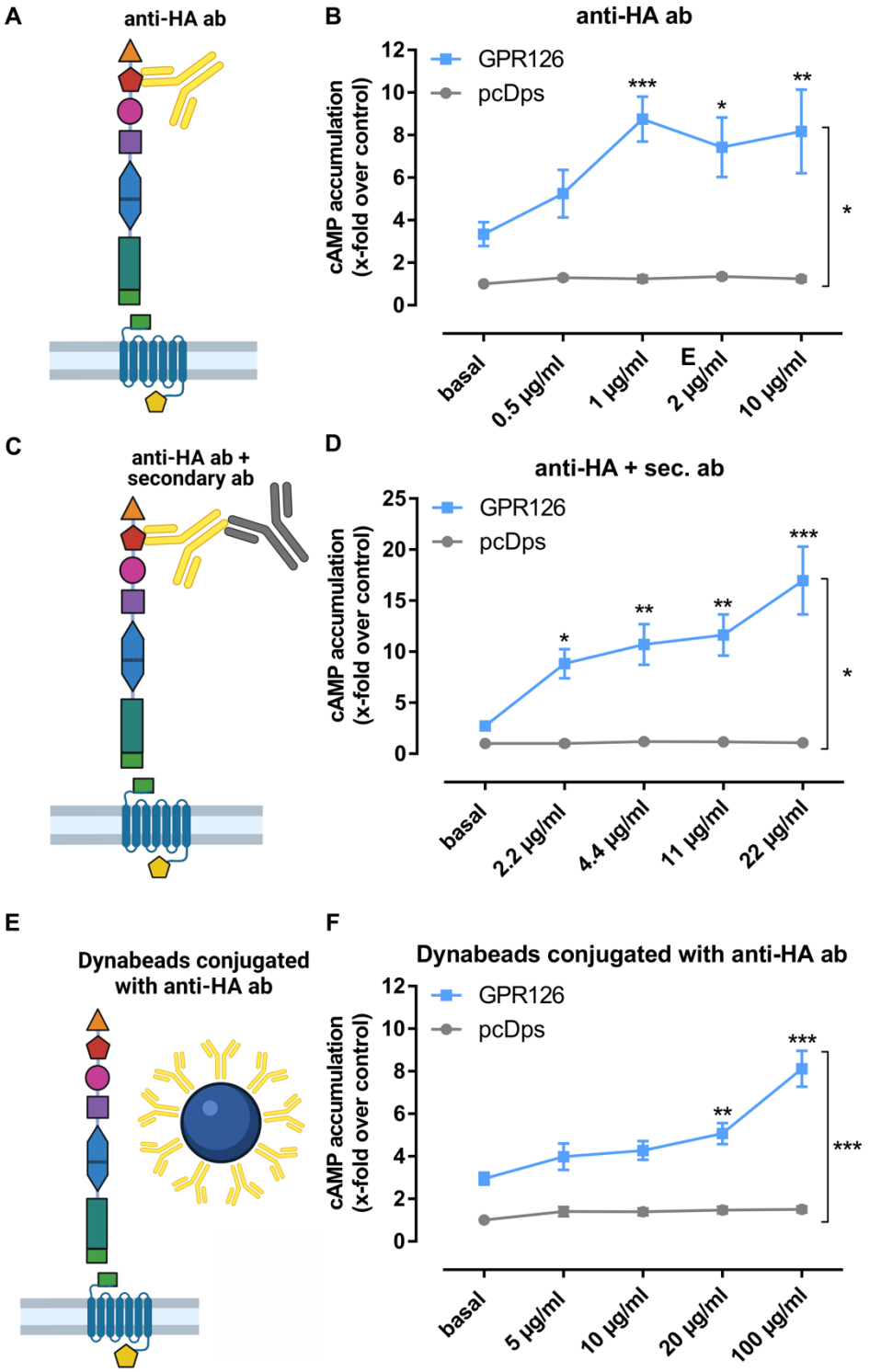

Figure 1. Antibodies against the N-terminus activate GPR126. (**A**) Schematic setup for the anti-HA antibody (anti-HA ab) stimulation of full-length WT GPR126 in cAMP accumulation assays (**B**). Different concentrations of anti-HA antibody were used to treat vector control (pcDps) and GPR126-transfected COS-7 cells (effect of construct $p = 0.0410$, effect of concentration $p < 0.0001$, interaction construct × concentration $p = 0.0506$; two-way ANOVA). Basal cAMP level in pcDps transfected cells: 8.9 ± 0.8 nM/well. (**C**, **D**) Amplification of cAMP signal of GPR126 with 1 µg/ml of anti-HA ab and subsequent incubation with different concentrations of secondary ab on vector control and GPR126-transfected COS-7 cells (effect of construct $p = 0.0104$, effect of

concentration $p < 0.0001$, interaction construct × concentration $p = 0.0072$; two-way ANOVA). Basal cAMP level in pcDps transfected cells: 4.2 ± 1.0 nM/well. (**E**, **F**) Paramagnetic Dynabeads® were conjugated with anti-HA ab and used in different concentrations for stimulation of vector control and GPR126-transfected COS-7 cells (effect of construct $p = 0.0001$, effect of concentration < 0.0001, interaction construct × concentration $p < 0.0001$; two-way ANOVA). Empty vector (pcDps) served as negative control. Basal cAMP level in pcDps transfected cells: 5.8 ± 0.4 nM/well. All data are given as means ± SEM of three – five independent experiments each performed in triplicates. Statistics were performed by applying a 2-way ANOVA followed by Dunnett post hoc analysis; *$p < 0.05$; **$p < 0.01$; ***$p < 0.001$. All significances given above individual points in the graphs show the result of the post hoc analysis. Schematic images were created with BioRender.com.

Anti-HA antibody-mediated activation depends on the *Stachel* sequence as well as GPS cleavage and is obliterated upon N-terminal prolongation

The N-terminus of GPR126 contains several functional domains, which can be subject to tissue-specific splicing (***Knierim et al., 2019***) and serve to interact with the known ligands collagen IV (***Paavola et al., 2014***), laminin 211 (***Petersen et al., 2015***) and prion protein (***Küffer et al., 2016***). To investigate their role in mechano-sensing, we used different N-terminal deletion mutants of GPR126, whose basal activity and expression levels were previously reported (***Petersen et al., 2015***). The constructs generated were: ΔCUB (lacking 109 aa compared to the WT), ΔPTX (lacking 206 aa) and ΔCUBΔPTX (lacking 315 aa). Additionally, we generated an N-terminally prolonged variant of GPR126 containing an mRuby-tag (236 aa prolongation compared to the WT) (Fig. 2A). Comparable protein expression levels of the mutants were demonstrated with cell surface and total ELISA assays in order to detect cell membrane and total protein expression, respectively (Suppl. Fig. S2A). The capability of receptor activation for each mutant was measured in cAMP accumulation assays using the synthetic GPR126 *Stachel* peptide as stimulus, thereby ensuring undisturbed signaling (Suppl. Fig. S2B). We stimulated these mutants with the same antibody-based setup as described in Fig. 1 and found that deletion of the CUB and PTX domains yields results highly similar to WT GPR126 (Fig. 2B). The N-terminally prolonged mRuby construct, despite showing WT-like expression and peptide activation (Suppl. Fig. S2A/B), could not be activated through antibodies (Fig. 2B).

The complex architecture of the N-terminus of GPR126 includes two cleavage sites; the GPCR proteolytic site (GPS) within the GAIN domain, and a furin site, located in the SEA domain (Fig. 2C). To analyze whether cleavage at either position may be required for antibody-mediated activation, we stimulated the furin-cleavage-deficient receptor mutant R468A, the GPS cleavage mutant H839R, and the double mutant R468A H838R with the same paradigm

178 (Fig. 2D). Prior to that, proper protein expression was confirmed with cell surface and total
179 ELISA (Suppl. Fig. S2A) and receptor activation via *Stachel* peptide stimulation was
180 demonstrated (Suppl. Fig. S2B). Proof of effective cleavage-deficiency was shown in Western
181 Blot with anti-HA antibody (Suppl. Fig. S2C). Interestingly, only the furin mutant R468A
182 retained increased cAMP levels upon antibody incubation, while no activation was seen for the
183 other mutants (Fig. 2D). These results suggest that furin cleavage is neglectable for antibody-
184 based mechano-activation, whereas GPS cleavage seems to be required. Similarly, mutation of
185 the *Stachel* sequence (F843A, Fig. 2C) obliterated antibody-induced activation of GPR126 (Fig.
186 2D), proving that the antibody does not directly activate the receptor but has to engage the
187 encrypted agonistic sequence.

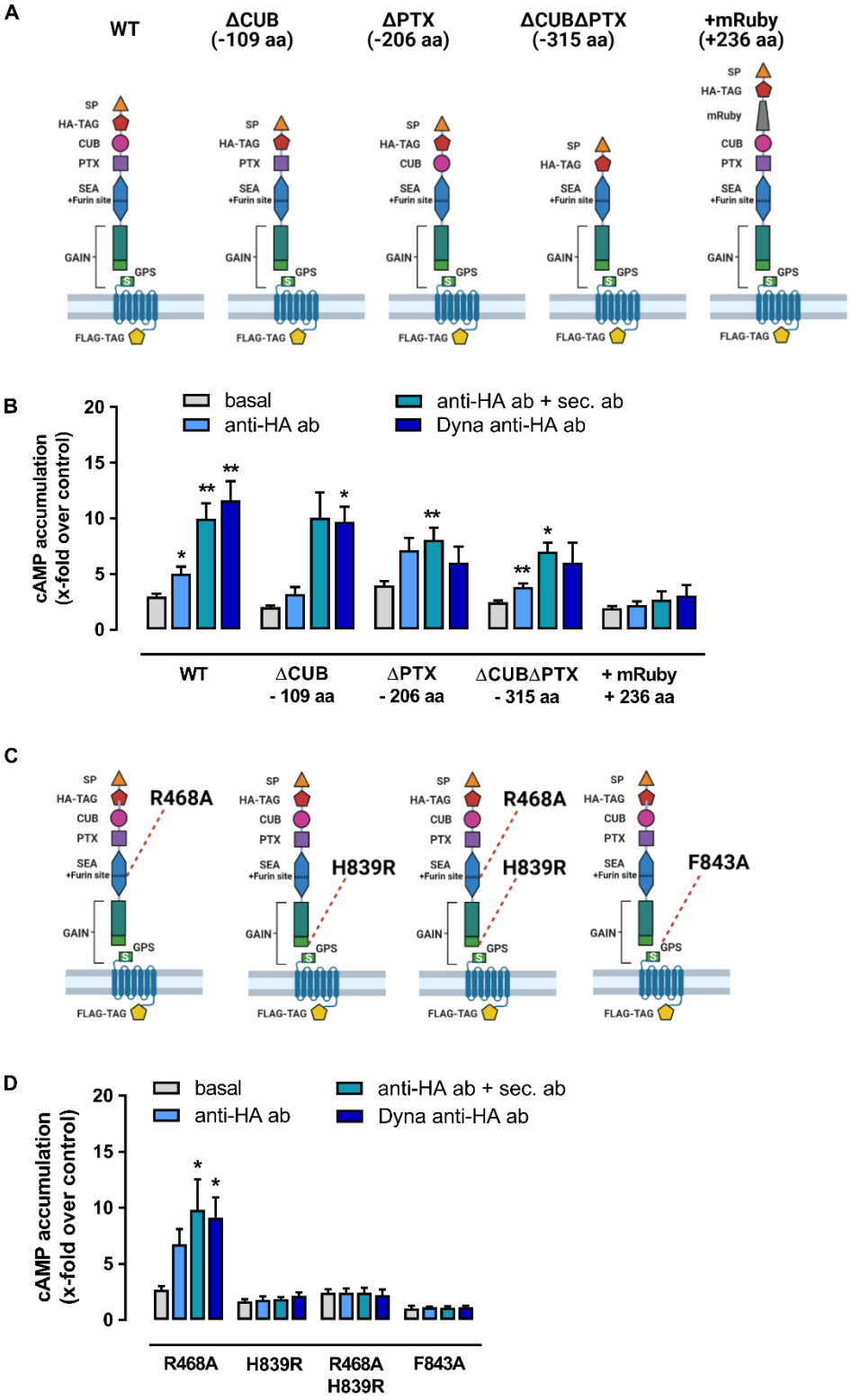

Figure 2. Antibody-mediated activation of GPR126 depends on autoproteolytic cleavage and is obliterated in a construct with an elongated N-terminus. (**A**) The domain architecture of the human GPR126 WT and respective mutants is depicted. The N-terminus contains the signal peptide (SP, orange triangle), a Complement C1r/C1s-Uegf-BMP1 domain (CUB, magenta oval), a pentraxin domain (PTX, purple square) and the Sperm protein, Enterokinase and Agrin (SEA) domain (blue hexagon) including the furin site. The highly conserved GAIN domain (green rectangle) contains the GPS, which is followed by the *Stachel* sequence (S). In our receptor constructs, we inserted a N-terminal hemagglutinin tag (HA-TAG, red pentagon) immediately distal to the signal

196 peptide a and a C-terminal Flag tag (FLAG-TAG, yellow pentagon) right before the Stop codon. (**B**) The receptor
197 variants were transfected into COS-7 cells and analyzed with the same antibody-based approach as used in Fig. 1.
198 (**C, D**) The furin-deficient receptor mutant R468A, the GPS cleavage mutant H839R, double mutant R468A
199 H838R, and the *Stachel* mutant F843A are displayed (**C**) and tested in cAMP assays (**D**). Images were created
200 with BioRender.com. Empty vector (pcDps) served as negative control (cAMP level: 4.3 ± 0.7 nM/well). Data are
201 given as mean ± SEM of three – eight different experiments each performed in triplicates. Statistics were
202 performed by applying a 1-way ANOVA followed by Dunnett post hoc analysis; *p < 0.05; **p < 0.01; ***p <
203 0.001. All shown statistical significances compare the condition to the basal cAMP accumulation of the same
204 construct.

205

206 **Anti HA antibody activates GPR126 through pushing and pulling forces**

207 In order to specify the mechanical forces needed to activate GPR126 through the anti-HA
208 antibody, we employed an atomic force microscopy (AFM) approach. We theorized that the
209 antibody could exert either pulling (through cross-linking) or pushing forces (through residing
210 on the cell layer) on the receptor, and that both can be quantified with AFM. To do so, tipless
211 AFM cantilevers were coated with anti-HA antibody using PEG linkers according to a well-
212 established protocol (***Ebner et al., 2007***). In contrast to cantilevers with a tip, this approach
213 allows for multiple antibodies to bind and thus interact with the cell surface. Therefore, the
214 mechanical force induced by the cantilever and mediated by the antibodies is applied to multiple
215 receptors expressed on the cell surface simultaneously. The coated cantilevers were then used
216 to apply pressure (pushing) or a force-clamp (pulling) to individual cells successfully co-
217 transfected with the given receptor construct and the Pink Flamindo cAMP sensor (***Harada et***
218 ***al., 2017***) (Fig. 3A). This setup allows for the simultaneous application of force and the
219 detection of changes in intracellular cAMP levels. Single cells within a confluent monolayer
220 were chosen for the measurements based on the detection of the GFP signal from the pUltra
221 vector, which allows for bicistronic expression of EGFP and GPR126 (***Lou et al., 2012***) and
222 the fluorescent signal from the Pink Flamindo cAMP sensor (***Harada et al., 2017***) (Suppl. Fig.
223 S3). Since COS-7 cells are not suited for AFM experiments due to their weak adherence to glass
224 coverslips, we used GripTite™ 293 MSR (HEK-GT) cells instead. Receptor cell surface
225 expression and activation in HEK-GT cells was confirmed prior to AFM experiments by ELISA
226 and cAMP accumulation assays, respectively (Suppl. Fig. S4). Relative possible Pink Flamindo
227 fluorescence changes upon stimulation of GPR126 with either forskolin, anti-HA antibody or
228 *Stachel* peptide pGPR126 are displayed in Suppl. Fig. S5.
229 The course of the cantilever deflection and therefore the force applied to the cell for the pushing
230 setup is depicted in Figures 3B and 3C. The cAMP-evoked changes in the Pink Flamindo

231 fluorescence were monitored by imaging right before the AFM cantilever applied pressure or a
232 pulling force and immediately after its retraction (Fig. 3B). A cantilever coated with human Fc-
233 protein instead of anti-HA antibodies was used as negative control.
234 When a pushing force of 1nN was applied over varying times, a significant increase in the Pink
235 Flamindo fluorescence signal could be observed compared to the negative control. This effect
236 got stronger and more significant over time (Fig. 3D: 180s and 300s) suggesting a time-
237 dependent increase in receptor activation (Fig. 3D). The control condition responded with a
238 reduction of cAMP sensor intensity over time, presumably due to bleaching effects by the AFM
239 detection laser. Having established that a significant increase in intracellular cAMP can be
240 achieved by pressure application via anti-HA antibody coated tips, we applied varying forces
241 over a constant time in order to quantify the strength of the pushing force needed to activate
242 GPR126 (Fig. 3E). Applying varying pushing forces (0.25nN - 1.5nN) with anti-HA antibody
243 coated tips over 60s lead to a highly significant increase in cAMP levels consistently over the
244 whole range of applied forces. When we performed the same experiment with the cleavage-
245 deficient mutant H839R (Fig. 3F), which showed no mechano-activation in cAMP
246 accumulation assays using antibodies and dynabeads (Figs. 2C, D), we observed no change in
247 the cAMP-mediated Pink Flamindo signal regardless of the pressure applied. This finding
248 suggested that pushing-mediated mechano-activation also requires autoproteolytic cleavage of
249 GPR126.
250 To further investigate the type and force of antibody-mediated mechano-activation of GPR126
251 we used the force-clamp setup, in which a pulling force is applied to the cell and receptors
252 (Figs. 3G, H). An Fc-control antibody-coated cantilever could not be used as a negative control
253 in this case, as it does not bind to the receptor or the HA-epitope and therefore no pulling forces
254 would be applied. Instead we compared the WT receptor to the mechano-insensitive H839R
255 mutant, which was still able to bind the anti-HA antibody. We applied varying pulling forces
256 (0.25 nN - 0.75 nN) over 60 seconds (Fig. 3I) and 300 seconds, as fold changes were very low
257 after the shorter pulling time period (Fig. 3J). We found the pulling forces to significantly
258 activate the receptor and observed a tendency towards lower pulling forces (0.25nN) being more
259 efficient than higher pulling forces (0.75nN).

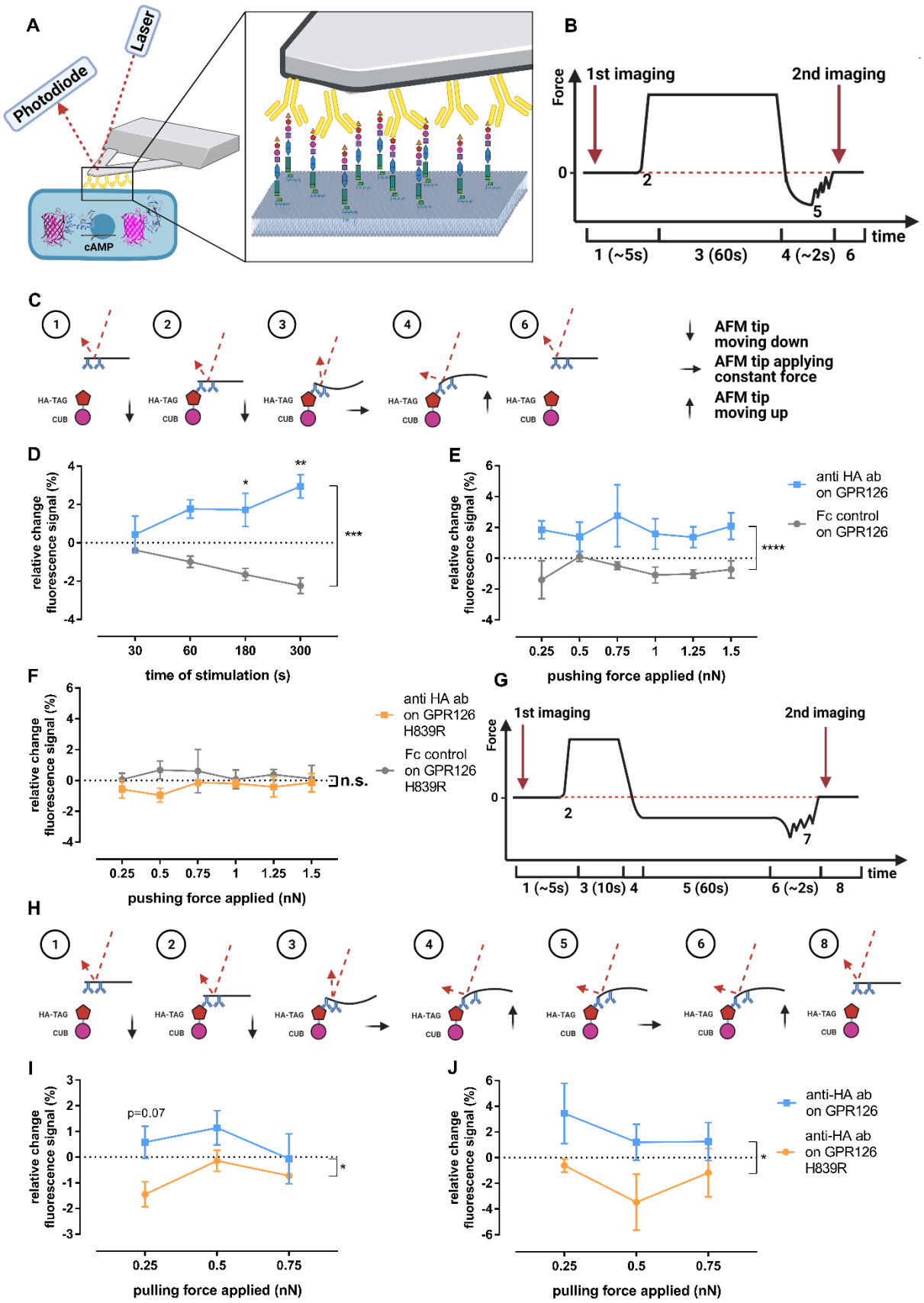

Figure 3. Mechano-activation of GPR126 via anti-HA antibodies. (**A**) Schematic AFM experiment setup with a coated tipless cantilever pressing on a cell co-transfected with GPR126 and the Pink Flamindo cAMP sensor. (**B, C**) Course of the AFM cantilever deflection during the pushing experiments and the forces applied to the

264 receptor and corresponding laser deflection: (1) Cantilever approaches cell; (2) Point of contact between cantilever
265 and cell; (3) Constant pressure being applied to the cell; (4) Cantilever is retracted from the cell; (5) Bindings
266 between cantilever and cell rupture; (6) All bindings are ruptured and the cantilever is back in its starting position.
267 (**D**) Changes in Pink Flamindo fluorescence intensity after applying a pushing force of 1 nN on the WT receptor
268 at different time points (effect of time $p = 0.775$, effect of coating $p = 0.0002$, interaction time × coating $p = 0.065$;
269 two-way ANOVA). (**E, F**) Changes in Pink Flamindo fluorescence intensity after applying indicated pushing
270 forces for 60s on the WT receptor (**E**) (effect of force applied $p = 0.878$, effect of coating $p < 0.001$, interaction
271 force × coating $p = 0.882$; two-way ANOVA) and the H839R mutant (**F**) (effect of force applied $p = 0.981$, effect
272 of coating $p = 0.0867$, interaction force × coating $p = 0.924$; two-way ANOVA). (**G, H)** Course of the AFM
273 cantilever deflection during the force clamp experiments and the forces applied to the receptor and corresponding
274 laser deflection:(1) Cantilever approaches cell; (2) Point of contact between cantilever and cell; (3) Initial pressure
275 being applied to allow binding between cantilever and cell; (4) Cantilever is retracted from the cell until the desired
276 pulling force is applied; (5) Constant pulling force is applied; (6) Cantilever is retracted from the cell completely;
277 (7) Bindings between cantilever and cell rupture; (8) All bindings are ruptured and the cantilever is back in its
278 starting position. Changes in Pink Flamindo fluorescence intensity after applying indicated pulling forces over (**I**)
279 60s (effect of force applied $p = 0.297$, effect of receptor variant $p = 0.0135$, interaction force × receptor variant p
280 $= 0.497$; two-way ANOVA) and (**J**) 300s (effect of force applied $p = 0.405$, effect of receptor variant $p = 0.0386$,
281 interaction force × receptor variant $p = 0.804$; two-way ANOVA). Data are given as means ± SEM of three-five
282 different experiments each measuring 3 individual cells for each force and time. Statistics were performed as 2-
283 way ANOVA followed by Tukey post hoc analysis; *$p < 0.05$; **$p<0.01$; *** $p<0.001$; **** $p<0.0001$.
284 Significances given at the right of each graph show the result of the ANOVA and significances given above
285 individual points in the graphs show the result of the post hoc analysis. Schematic images (A-C and G-H) were
286 created with BioRender.com. The Pink Flamindo depiction in A was taken from (***Harada et al., 2017***).

287

288 **Endogenous ligands of GPR126 convey a highly specific type of mechano-activation**

289 Having established a reliable way to measure activation-inducing forces on GPR126, we set to
290 investigate the forces needed to stimulate GPR126 using its natural ligands. Several ligands
291 have been shown to modulate GPR126 activity (Fig. 4A): for example collagen IV has been
292 described as directly activating ligand (***Paavola et al., 2014***), which could be interpreted as a
293 pushing force on the receptor as it 'sits' on it. Laminin 211 on the other hand was reported to
294 require mechanical stimuli such as shaking or vibration to induce cAMP signaling (***Petersen et***
295 ***al., 2015***), which could be a proxy for pulling forces. To test these assumptions, tipless AFM
296 cantilevers were coated with collagen IV or laminin 211. Again, all experiments were
297 performed on HEK-GT cells co-transfected with Pink Flamindo and either WT GPR126 or the
298 GPR126 H839R mutant. The empty pUltra vector was used as a negative control.

299

Interestingly, when pushing at WT GPR126 transfected cells with a collagen IV-coated cantilever (Fig. 4B), it took specifically 1 nN to induce a significant increase in cAMP levels (Fig. 4C). Lower or higher pressure did not activate the receptor. Again, GPR126 H839R could not be activated through this mechanical stimulus. Applying pulling forces with collagen IV did not produce any significant changes in the Pink Flamindo fluorescence signal for neither the WT receptor nor the cleavage-deficient mutant (Fig. 4D). The Laminin 211-coated cantilever (Fig. 4E) did not activate GPR126 through pushing (Fig. 4F), but a significant increase in the Pink Flamindo fluorescence signal was seen in the force-clamp setup when applying a pulling force of 0.75 nN (Fig. 4G). Lower pulling forces were not sufficient to activate the receptor.

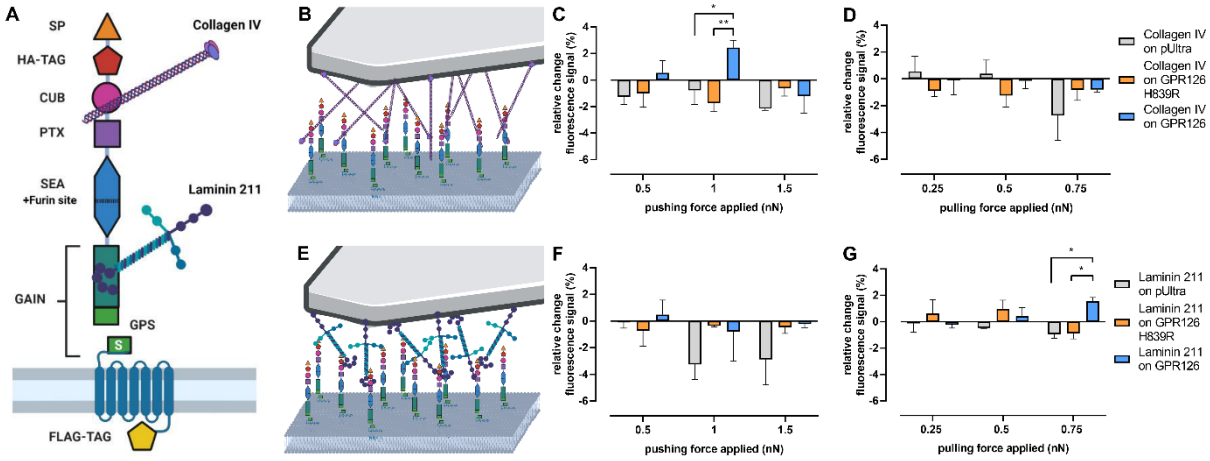

Figure 4. Mechano-activation of GPR126 via its ligands. (**A**) The domain architecture of human GPR126 with the binding sites of its ligands, collagen IV and laminin 211, is depicted. (**B, E**) Schematic demonstrating the AFM setup with collagen IV (**B**) and laminin 211 (**E**). (**C, D**) Changes in Pink Flamindo fluorescence intensity after applying a varying pushing (**C**) or pulling (**D**) force over 60s with a collagen IV-coated cantilever. (**F, G**) Changes in Pink Flamindo fluorescence intensity after applying a pushing (**F**) or pulling (**G**) force over 60s with a laminin 211-coated cantilever. Data are given as means ± SEM of three different experiments, each measuring 3 individual cells for each force. Statistics were performed as 2-way ANOVA (**C**: Interaction: p=0.029; **G**: Interaction: p=0,025; **D, F**: n.s.) in combination with Tukey post hoc analysis; *p < 0.05; **p < 0.01. Significances in the graphs show the results of the post hoc analysis. Schematic images were created with BioRender.

Discussion

The aGPCR GPR126 can be activated through different mechanisms, including agonistic *Stachel* sequence-derived peptides (***Liebscher et al., 2014***), its ligands collagen IV (***Paavola et al., 2014***), laminin 211 (***Petersen et al., 2015***) and prion protein (***Küffer et al., 2016***), the small

326 molecule compound apomorphine (***Bradley et al., 2019***) and mechanical stimuli such as
327 vibration or shaking (***Petersen et al., 2015***). Yet, all of these activators lack specificity for
328 GPR126, which hampers their usefulness as tools for *in vivo* experiments or potential
329 therapeutics. The agonistic peptide pGPR126 can for example cross-activate the aGPCR
330 GPR64/ADGRG2 (***Demberg et al., 2017***), while the ECM molecules collagen and laminin can
331 also bind and activate integrins (***Keely et al., 1995***) and apomorphin is an agonist on dopamine
332 receptors (***Millan et al., 2002***). In this study we show that a commonly used monoclonal
333 antibody targeting an N-terminal HA epitope can serve as an activator of GPR126. This
334 activation is further increased by adding a secondary antibody. Paramagnetic Dynabeads®
335 coated with the anti-HA antibody could also stimulate cAMP production in GPR126 transfected
336 cells, however to a similar extend as the anti-HA ab alone, while a magnetic field placed below
337 the cell culture well did not alter this effect. Future studies with a stronger or alternating
338 magnetic field might be able to trigger GPR126 activation.
339 Antibody-mediated GPCR activation is a known phenomenon. For example, in several disease
340 contexts, autoantibodies target GPCRs, such as the thyroid stimulating hormone receptor,
341 calcium-sensing receptor and muscarinic M1 and M2 receptors (***Unal et al., 2012***). However,
342 here we use antibodies to experimentally modulate aGPCR signaling and create a new toolbox
343 that allows us to study receptor activation. Previously, the aGPCRs EMR2 and GPR56 were
344 shown to be activated through antibodies targeting the receptors' N-termini (***Bhudia et al.,***
345 ***2020; Chatterjee et al., 2021; Yona et al., 2008***). In the absence of known antibodies against
346 the N-terminus of GPR126, we introduced the HA epitope into the N-terminus of GPR126 and
347 employed a commercial anti-HA antibody to modulate signalling. While the effect is elicited
348 using an exogenous epitope and its cognate antibody, it nonetheless illustrates the principle that
349 antibody binding to the N-terminus of GPR126 influences receptor activation, similar to other
350 aGPCRs. Ultimately, development of antibodies against the native amino acid sequences of
351 GPR126 will pave the way towards further basic experimentation and therapeutic applications.
352
353 When studying aGPCR activation by ligands or antibodies, splice variants have to be
354 considered, since the complex exon-intron composition results in a large subset of functionally
355 divergent receptors. As an example, activation of GPR56 through an antibody targeting the
356 GAIN domain is dependent on a Serine–Threonine–Proline-rich (STP) region, which otherwise
357 does not influence basal signaling levels of the receptor (***Chatterjee et al., 2021***). In the case of
358 GPR126, alternative splicing influences the domain composition of the N-terminus (***Knierim***
359 ***et al., 2019***). Within the N-terminus, the CUB/PTX domain is of functional relevance as it

360 serves as point of interaction for collagen IV (***Paavola et al., 2014***), yet, for anti-HA antibody-
361 mediated mechano-activation it appears to be neglectable. This would decrease considerably a
362 potential variability of the antibody-induced response when used in a physiologic setting. In
363 contrast, elongating the receptor's N-terminus through the addition of a fluorescent protein
364 abolishes this activation. Similar observations have been made for the adhesion GPCR dCIRL,
365 where elongation of the N-terminus reduces the response to mechanical stimuli (***Scholz et al.,***
366 ***2017***). Thus, large artificial N-terminal domains influence signaling properties, even when they
367 do not act as binding sites for the activating antibodies. It is currently unknown whether this is
368 due to the simple change in length or altered three-dimensional structure of the N-terminus.
369
370 We have further investigated the role of cleavage in antibody-mediated activation of GPR126.
371 The receptor's N-terminus harbors a furin site located in the SEA domain, and an
372 autoproteolytic cleavage motif (GPS) within the GAIN domain. We find that abolishing furin
373 cleavage does not affect response to antibody-mediated activation while abrogation of the GPS
374 cleavage blunts the effect of the antibody. This observation may support the idea that NTF-CTF
375 dissociation is an integral part of the receptor's response to the antibody treatment, and its
376 activation in general. However, this concept may be receptor-specific rather than generalizable
377 to all aGPCRs. For example, antibody-mediated activation of GPR56 (***Chatterjee et al., 2021***)
378 and mechano-sensation of latrophilin (***Scholz et al., 2015***) are not affected by mutations of their
379 GPS cleavage motifs. Thus, it seems that autoproteolysis at the GPS serves distinct purposes
380 among different receptors. Our experiments also demonstrate that antibody-mediated activation
381 of GPR126 depends on the endogenous encrypted agonist, the *Stachel* sequence. This,
382 combined with the finding that the effect requires autoproteolytic cleavage, suggest the
383 underlying mechanism involves high-affinity antibody binding to the N-terminus, induced
384 dissociation of the NTF and CTF, and a CTF configuration that allows the *Stachel* sequence to
385 act as the endogenous agonist.
386 In many ways, the activation of GPR126 through the anti-HA antibody resembles characteristic
387 features seen for the activation through mechanical forces, such as vibration and shaking,
388 including the dependence on the tethered agonist and cleavage (***Petersen et al., 2015***), and the
389 negative impact of N-terminal elongation (***Scholz et al., 2015***). We, therefore, hypothesize that
390 antibody-induced GPR126 activation mechanistically overlaps with mechano-activation.
391 While mechano-activation has been widely accepted as a component of aGPCR activation,
392 there are still unanswered questions with regard to the magnitude and type of forces needed. To
393 begin answering these questions in the case of GPR126, we employed an atomic force

394 microscopy approach in combination with fluorescent cAMP imaging. Using an antibody-
395 coated cantilever, we found that tonic forces, whether pushing or pulling, as little as 0.25 nN
396 induce receptor activation. This might explain, why we did not detect any additional activation
397 when placing a magnet below the cell culture plate, as the Dynabeads® alone could push
398 enough to reach saturating effects. The combination with a secondary antibody could enhance
399 GPR126 activation through an increased cross-linking of receptors, which would combine
400 pushing and pulling forces.
401 The push and pulling effects depend on autoproteolytic cleavage, similar to the effects of the
402 antibody alone and antibody-coated beads. To ensure that applying pushing forces onto cells is
403 not a non-specific event, we showed that there is no change in cAMP levels of GPR126-
404 expressing cells when the cantilever is coated with an Fc fragment. Even though published
405 single molecule AFM analysis indicated that forces in the pN range are sufficient to unfold
406 GPCRs such as the protease-activated receptor 1 (PAR1) (***Alsteens et al., 2015***), there is no
407 indication that the pulling forces exerted in our experimental paradigm would lead to such a
408 structural disruption, since we use a tipless cantilever that binds multiple antibodies, thereby
409 interacting with several receptors at the same time. As the size of the adhesive interface and
410 traction forces display a linear relationship, one would expect a much higher traction force
411 needed to unfold GPR126 in our setup. A comparable force requirement could be deduced from
412 an experiment that studied the interaction strength between fibronectin-coated beads and cell
413 surface. The forces needed to disrupt this interaction were > 2 nN (***Mierke et al., 2008***), which
414 is much higher than the pulling force (0.25 nN) needed to activate GPR126. Therefore, we
415 conclude that the increase in cAMP is specifically mediated by a pulling force on the intact
416 receptor and does not present an artefact due to structural destruction of the receptor.
417 These pulling forces are also below the traction forces that are normally transmitted by cell
418 adhesions to the surrounding extracellular matrix (ECM) (1 – 10 nN) (***Balaban et al., 2001***),
419 indicating that even small changes can be detected by an aGPCR as it is embedded within the
420 ECM. The forces mediated by two known ligands of GPR126 that change intracellular cAMP
421 are indeed within this physiologic force range. We found that collagen IV requires a pushing
422 force of 1 nN to raise cAMP, while Laminin 211 activates GPR126 upon pulling with a force
423 of 0.75 nN. Our results also match observations from previous signalling assays, where
424 incubation of GPR126-expressing cells with laminin 211 requires the addition of vibration or
425 shaking to induce an increase in cAMP (***Petersen et al., 2015***). Both activation patterns fit the
426 physiological setting for these ligands in the process of myelination (***Bunge et al., 1990***).
427 Schwann progenitor cells require low cAMP levels to continue proliferation. This proliferation

occurs in the same time window as the production of the first basal membrane components, among them laminin 211. Only when there are sufficient amounts of laminin 211 does it start polymerizing. The polymer, in turn, is believed to exert a traction force on GPR126 leading to a burst of cAMP, which eventually switches the Schwann progenitor cells from the proliferative to a differentiated state and leads to myelination (***Bacallao and Monje, 2015; Petersen et al., 2015***). Collagen IV is then added onto the laminin 211-based membrane to stabilize it. The presence of collagen IV, through its activation of GPR126, maintains the higher cAMP levels associated with Schwann cell differentiation and myelination.

In summary, we were able to define the mechanical forces required to induce ligand and antibody-mediated activation of GPR126 *in vitro,* where the antibody reproduces both ways of mechanical stimulation employed by the endogenous ligands. Our findings emphasize the role of mechano-activation in translating interaction of GPR126 with ECM components to receptor activation and signalling and provide a tool to study these in a simplified but modifiable antibody-based setup.

443 **Materials and Methods**

444 If not stated otherwise, all standard substances were purchased from Sigma Aldrich
445 (Taufkirchen, Germany), Merck (Darmstadt, Germany), and C. Roth GmbH (Karlsruhe,
446 Germany). Cell culture material was obtained from ThermoFisher Scientific (Schwerte,
447 Germany) and primers were obtained from Microsynth Seqlab GmbH (Göttingen, Germany).
448

449 The constructs of human GPR126 and ΔCUB, ΔPTX, ΔCUBΔPTX mutants have been
450 described previously (***Liebscher et al., 2014; Mogha et al., 2013; Petersen et al., 2015***). Point
451 mutations for R468A and H839R mutants were inserted by quick change mutagenesis. In brief,
452 plasmid DNA was amplified with PCR and then digested with DpnI restriction enzyme for 4 h
453 at 37 °C prior heat shock transformation in *E. coli*. The mRuby epitope was inserted in the
454 human GPR126 construct after the hemagglutinin (HA) epitope by a PCR-based site-directed
455 mutagenesis and fragment replacement strategy. The sequences of all generated mutants of
456 human GPR126 were verified by Sanger sequencing (Microsynth Seqlab, Göttingen,
457 Germany).
458 The GPR126/pULTRA construct was generated using One-step isothermal DNA assembly
459 (***Gibson et al., 2009***). The reaction buffer was prepared according to protocol. All enzymes
460 were acquired from NEB: T5 exonuclease (M0363), Taq DNA Ligase (M0208) and Phusion
461 DNA Polymerase (M0530). The wt receptor DNA for the assembly was obtained via PCR using
462 the previously described construct of the full-length human GPR126 in the pcDps vector
463 (***Liebscher et al., 2014***). The pULTRA (pUltra was a gift from Malcolm Moore, Addgene
464 plasmid #24129, (***Lou et al., 2012***)) vector was restriction digested using Xba1 (NEB, R0145).
465

466 ***In vitro* functional assays**
467 The human N- and C-terminally tagged GPR126 was heterologously expressed in COS-7 cells
468 grown in Dulbecco's minimum essential medium (DMEM) supplemented with 10 % fetal
469 bovine serum (FBS), 100 units/ml penicillin, and 100 µg/ml streptomycin or the GripTite 293
470 MSR Cell Line (ThermoFisher Scientific) (HEK-GT) grown in DMEM supplemented with 10
471 % fetal bovine serum, 1 % G418 (ThermoFisher, 10131035) and 1 % Non-Essential Amino
472 Acids (ThermoFisher, 11140050) at 37 °C and 5 % CO_2 in a humidified atmosphere. For the
473 establishment of antibody-based assays, conjugated Dynabead stimulation in a magnetic field
474 and enzyme-linked immunosorbent assay (ELISA), cells were split into 48-well plates (3×10^4
475 cells/well for COS-7 or 1.3×10^5 cells/well for HEK-GT) or into 6-well plates for total ELISA

476 (3×10^5 cells/well for COS-7 or 1.5×10^6 cells/well for HEK-GT). For peptide stimulation, cells
477 were split into 96-well plates (1.5×10^4 cells/well for COS-7 or 4.5×10^4/well for HEK-GT). For
478 Western Blot analysis, cells were split into 24-well plates (6×10^4 cells/well for COS-7).
479 Transfection was done with Lipofectamine 2000 (ThermoFisher Scientific) according to the
480 manufacturer's protocol. 50 ng (96-well plates) or 500 ng (48-well plates) of receptor plasmid
481 DNA/well were used for cAMP accumulation assays. To perform cAMP accumulation assays,
482 48 h after transfection, GPR126 and empty vector-transfected cells were stimulated with the
483 indicated concentrations of anti-HA antibody (H3663, stock concentration 1 mg/ml, Sigma-
484 Aldrich) or anti-FLAG antibody (F1804, Sigma-Aldrich) in DMEM for 1 h, followed by
485 incubation with 3-isobutylmethyl-xanthine (1 mM)-containing medium or including the
486 secondary antibody anti-mouse IgG (Fc specific, M2650, Sigma-Aldrich) for 30 min. To
487 perform mechanical forces on transfected COS-7 cells, cells were treated with vibration
488 frequency of 17 Hz for 30 min. For peptide stimulation, *Stachel*-sequence derived peptide was
489 diluted in IBMX-containing medium. Peptide solution from purified powder was achieved by
490 preparing a 100 mM in 100 % DMSO solution, which was further diluted into 10 mM stocks
491 using a 50 mM, pH 8 Tris buffer and finally pH controlled. Peptide concentrations used in
492 assays are 1 mM. The 1 mM peptide solution contains 1 % DMSO and 10 % of Tris buffer used
493 for dilution. After stimulation cells were lysed in LI buffer (PerkinElmer Rodgau, Germany)
494 and kept frozen at −20 °C until measurement. To measure cAMP concentration, the Alpha
495 Screen cAMP assay kit (PerkinElmer) was used according to the manufacturer's protocol. The
496 accumulated cAMP was measured in 384-well white OptiPlate microplates (PerkinElmer) with
497 the EnVision Multilabel Reader (PerkinElmer). Super paramagnetic Dynabeads® (14311D,
498 ThermoFisher Scientific) were conjugated with anti HA antibody according to the
499 manufacturer's protocol. The magnetic stimulator was created via embedding N45 NdFeB
500 magnets (https://www.supermagnete.de/data_sheet_S-08-05-N.pdf) into a custom 3D printed
501 holder matching the outer diameter of a corresponding cell culture plate.
502 To estimate cell surface expression of receptors carrying an N-terminal HA tag, an indirect
503 cellular enzyme-linked immunosorbent assay (ELISA) was used (***Schöneberg et al., 1998***).
504 The HEK-GT cells used for cAMP accumulation assays and ELISA were not only transfected
505 with the receptor plasmid DNA but the Pink Flamindo cAMP sensor as well to account for
506 changes in expression and activatability due to the co-transfection used in the AFM
507 experiments.
508
509 **Western Blot**

510 COS-7 cells were transfected with either empty pcDps vector, or GPR126, GPR126 R468A and
511 GPR126 R468A/H839R using the standard protocols described earlier. Every other transfected
512 construct was incubated with primary anti-HA antibody for an hour as explained before. Cells
513 were lysed with the addition of 300 µl of 2x SDS loading dye. After freeze thaw cycling the
514 lysates were run on a 10% SDS-PAGE gel, followed by western blotting. The membranes were
515 blocked for 1h with 5% non-fat dry milk in TBST buffer, washed 3 times with TBST buffer
516 and incubated over night with either primary antibody (rabbit HA and GAPDH antibody, cell
517 signaling). The following day, membranes were again washed with TBST buffer and incubated
518 with the secondary anti-rabbit antibody, which has an HRP conjugation (cell signaling) for 1h
519 at room temperature. This was followed by three additional washing steps with TBST buffer.
520 Membranes were wetted with SuperSignal West Pico PLUS Chemiluminescent Substrate
521 (ThermoFisher Scientific) to visualize protein bands, which were imaged using the Bio-Rad
522 Gel Doc Imager.
523
524 **AFM**
525 For all AFM experiments, HEK-GT cells were cultured at the same conditions as for the *in vitro*
526 functional assays. Cells were seeded on 24 mm glass coverslips (coated with Poly-L-Lysin
527 (Sigma-Aldrich, P4707), (1 % PLL solution incubated at 37 °C for 5 minutes then washed with
528 PBS and dried under a sterile hood) in 6-well plates ($1.5x10^6$ cells/well) and co-transfected with
529 the cAMP sensor Pink Flamindo (Addgene plasmid #102356) and either empty vector or the
530 given GPR126 construct in the pULTRA vector on the next day using Lipofectamine 2000
531 according to the manufacturer's protocol. The media was changed to the described culture
532 media ~24h after transfection and AFM measurements took place ~48h after transfection: the
533 coverslips were transferred into a 35mm cell culture dish and washed with DMEM without
534 phenol red 3 three times and placed into AFM coverslip holders. 750µl culture media without
535 phenol red was added and the cells were stored at 37 °C and 5 % CO_2 until right before the
536 measurements took place.
537 Tipless silicon nitride AFM cantilevers (NanoWorld, PNP-TR-TL) were coated with
538 monoclonal anti-HA antibodies produced in mouse (H3663, Sigma-Aldrich) or Fc-control for
539 the antibody-based mechano-activation experiments using flexible PEG spacers as described
540 before (***Ebner et al., 2007***). Recombinant human Fc was expressed by transfected Chinese
541 hamster ovary (CHO) cells, supernatant was collected and purification was done via His-tag
542 using HisLink Protein Purification Resin (V8823, Promega) according to manufacturer's
543 instructions. Protein purity was confirmed by Western blot analysis. For the ligand-based

544 mechano-activation experiments, tipless silicon nitride AFM cantilevers were washed twice in
545 Chloroform and dried. The cantilevers were then placed into a collagen IV (C6745, Sigma
546 Aldrich) or laminin-211 (LN221, BioLamina, Sundbyberg, Sweden) solution (0.15 mg/ml) and
547 incubated at 4 °C overnight. The next day the cantilevers were washed in HBSS twice and
548 stored in HBSS at 4 °C until use.
549 Atomic Force Microscopy (AFM) measurements were performed using a Nanowizard IV AFM
550 (Bruker, Billerica, MA) mounted on an IX 83 inverted optical microscope equipped with a 63x
551 PL APO NA 1.42 oil objective (both Olympus Lifes Sciences, Wallisellen, Switzerland) and
552 coupled to a X-Cite Exacte Light source (Excelitas Technologies, Waltham, MA).
553 Cantilevers were calibrated using the thermal noise method according to (***Slattery et al., 2013***).
554 Successfully double-transfected cells were identified by the GFP from the pULTRA vector and
555 the Pink Flamindo fluorescence signal. The cell was then imaged three times in the following
556 order: Brightfield, GFP and Pink Flamindo using a Zyla sCMOS camera (Andor Technology,
557 Belfast, Northern Ireland). The AFM cantilever was then placed centrally on the cell and
558 approached until contacting the cell surface. Proper positioning was verified by a brightfield
559 image and the baseline Pink Flamindo signal was recorded. During stimulation all light sources
560 except the AFM laser were turned off. Immediately after the stimulation was finished, another
561 image of the Pink Flamindo signal was obtained using the same exposure time as before.
562 For force clamp measurements, the cantilevers were initially pressed onto the cell with a force
563 of 1 nN for 5 seconds in order to allow antibody/ligands and receptor to bind. The cantilever
564 was then retracted (1 µm/s) until the desired clamp force was reached. This value was kept
565 constant for the indicated times before the cantilever was fully retracted.
566 Extend and Retract length was 15 µm and Extend and Retract speed was 5 µm/s for all
567 experiments.
568 For analysis, the Pink Flamindo images made before and after the stimulation were compared
569 by measuring the mean intensity of a rectangular area on the stimulated cell using Fiji Image J
570 (***Schindelin et al., 2012***). To account for variations affecting all cells independently from the
571 stimulation, such as bleaching, a rectangular area was measured on five other cells that were
572 not touched by the cantilever but expressed Pink Flamindo. The average of the change in these
573 5 reference cells was subtracted from the measured change in the stimulated cell to isolate the
574 effect the AFM cantilever stimulation has on the receptor-transfected cell (Suppl. Fig. S3).
575
576 To evaluate the mechano-independent changes of the Pink Flamindo fluorescence signal, HEK-
577 GT cells were split into 96-well plates (4.5×10^4/well) and transfected the following day analog

578 to the cAMP accumulation assays described earlier. Two days after transfection the media was
579 removed from the wells and 40µl of DMEM without phenol-red were added to each well. Then
580 the GFP signal (transfection control) as well as the Pink Flamindo fluorescence signal were
581 imaged using a Celigo Image Cytometer (Nexcelom Bioscience). Forskolin, pGPR126 and anti-
582 HA ab diluted in DMEM without phenol-red were added to a final volume of 50 µl/well and
583 following concentrations: 10 µM forskolin, 1 µM anti-HA ab and 1 mM pGPR126. The cells
584 were imaged again 60 s after addition of the respective stimulus and the intensity of the Pink
585 Flamindo signal beforehand and afterwards was compared.
586

587 **Data Analysis**

588 Receptor expression and activation were analyzed using, 1- and 2-way ANOVA as well as t-
589 test as indicated at each figure legend. p values < 0.05 were considered statistically significant
590 (*p<0.05; **p<0.01; ***p<0.001). All statistical analyses were performed by GraphPad Prism
591 version 6.00 for Windows (GraphPad Software, Inc. (La Jolla, USA)) or Microsoft Excel 2016
592 (Microsoft Corporation (Redmond, USA)).
593

594 **Acknowledgements**

595 Our research is funded by the German Research Foundation (CRC1052 project number
596 209933838 to IL, CRC1423 project number 421152132 B05 to IL, FOR2149 project number
597 246212759, P5) to IL and (STE 2843/1-1 project number) to GS. Further funding comes from
598 the European Union (European Social Fund) to IL and the Swiss National Science Foundation
599 (SNF 310030_197764/1) to VS. Further support was provided by the junior research grant by
600 the Medical Faculty, Leipzig University to CW and by the COST association providing an
601 STSM grant within the COST action CA18240 to JM. DGP was supported by NIH/NINDS R01
602 NS102665, NYSTEM (NY State Stem Cell Science) IIRP C32595GG, NIH/NIBIB R01
603 EB028774, NYU Grossman School of Medicine, and DFG FOR2149.

604 **Author Contributions**

605 JM, CW, CS, VS, DGP and IL designed the research plan. JF, GS, JM, HK, SB and CW
606 performed the experiments. JF, GS, JM, SB, CW and IL analyzed results. JM, CW and IL wrote
607 the paper with input from all authors. All authors edited and approved of the manuscript.
608

609 **Competing interests**

610 The authors declare no competing interest.

611

612 **References**

613 **Alsteens D**, Pfreundschuh M, Zhang C, Spoerri PM, Coughlin SR, Kobilka BK, Müller DJ. 2015.
614 Imaging G protein-coupled receptors while quantifying their ligand-binding free-energy landscape.
615 *Nature Methods* **12**:845–851.

616 **Arac D**, Boucard AA, Bolliger MF, Nguyen J, Soltis SM, Südhof TC, Brunger AT. 2012. A novel
617 evolutionarily conserved domain of cell-adhesion GPCRs mediates autoproteolysis. *The EMBO*
618 *Journal* **31**:1364–1378.

619 **Bacallao K**, Monje PV. 2015. Requirement of cAMP signaling for Schwann cell differentiation restricts
620 the onset of myelination. *PloS One* **10**:e0116948.

621 **Balaban NQ**, Schwarz US, Riveline D, Goichberg P, Tzur G, Sabanay I, Mahalu D, Safran S,
622 Bershadsky A, Addadi L, Geiger B. 2001. Force and focal adhesion assembly: a close relationship
623 studied using elastic micropatterned substrates. *Nature Cell Biology* **3**:466–472.

624 **Bhudia N**, Desai S, King N, Ancellin N, Grillot D, Barnes AA, Dowell SJ. 2020. G Protein-Coupling
625 of Adhesion GPCRs ADGRE2/EMR2 and ADGRE5/CD97, and Activation of G Protein Signalling
626 by an Anti-EMR2 Antibody. *Scientific Reports* **10**:1004.

627 **Bradley EC**, Cunningham RL, Wilde C, Morgan RK, Klug EA, Letcher SM, Schöneberg T, Monk KR,
628 Liebscher I, Petersen SC. 2019. In vivo identification of small molecules mediating Gpr126/Adgrg6
629 signaling during Schwann cell development. *Annals of the New York Academy of Sciences* **1456**:44–
630 63.

631 **Bunge MB**, Clark MB, Dean AC, Eldridge CF, Bunge RP. 1990. Schwann cell function depends upon
632 axonal signals and basal lamina components. *Annals of the New York Academy of Sciences* **580**:281–
633 287.

634 **Chatterjee T**, Zhang S, Posey TA, Jacob J, Wu L, Yu W, Francisco LE, Liu QJ, Carmon KS. 2021.
635 Anti-GPR56 monoclonal antibody potentiates GPR56-mediated Src-Fak signaling to modulate cell
636 adhesion. *The Journal of Biological Chemistry* **296**:100261.

637 **Demberg LM**, Winkler J, Wilde C, Simon K-U, Schön J, Rothemund S, Schöneberg T, Prömel S,
638 Liebscher I. 2017. Activation of Adhesion G Protein-coupled Receptors: AGONIST SPECIFICITY
639 OF STACHEL SEQUENCE-DERIVED PEPTIDES. *The Journal of Biological Chemistry* **292**:4383–
640 4394.

641 **Diamantopoulou E**, Baxendale S, La Vega León A de, Asad A, Holdsworth CJ, Abbas L, Gillet VJ,
642 Wiggin GR, Whitfield TT. 2019. Identification of compounds that rescue otic and myelination defects
643 in the zebrafish adgrg6 (gpr126) mutant. *eLife* **8**.

644 **Ebner A**, Wildling L, Kamruzzahan ASM, Rankl C, Wruss J, Hahn CD, Hölzl M, Zhu R, Kienberger
645 F, Blaas D, Hinterdorfer P, Gruber HJ. 2007. A new, simple method for linking of antibodies to
646 atomic force microscopy tips. *Bioconjugate Chemistry* **18**:1176–1184.

Gibson DG, Young L, Chuang R-Y, Venter JC, Hutchison CA, Smith HO. 2009. Enzymatic assembly of DNA molecules up to several hundred kilobases. *Nature Methods* **6**:343–345.

Harada K, Ito M, Wang X, Tanaka M, Wongso D, Konno A, Hirai H, Hirase H, Tsuboi T, Kitaguchi T. 2017. Red fluorescent protein-based cAMP indicator applicable to optogenetics and in vivo imaging. *Scientific Reports* **7**:7351.

Karner CM, Long F, Solnica-Krezel L, Monk KR, Gray RS. 2015. Gpr126/Adgrg6 deletion in cartilage models idiopathic scoliosis and pectus excavatum in mice. *Human Molecular Genetics* **24**:4365–4373.

Keely PJ, Wu JE, Santoro SA. 1995. The spatial and temporal expression of the alpha 2 beta 1 integrin and its ligands, collagen I, collagen IV, and laminin, suggest important roles in mouse mammary morphogenesis. *Differentiation* **59**:1–13.

Knierim AB, Röthe J, Çakir MV, Lede V, Wilde C, Liebscher I, Thor D, Schöneberg T. 2019. Genetic basis of functional variability in adhesion G protein-coupled receptors. *Scientific Reports* **9**:11036.

Kou I, Takahashi Y, Johnson TA, Takahashi A, Guo L, Dai J, Qiu X, Sharma S, Takimoto A, Ogura Y, Jiang H, Yan H, Kono K, Kawakami N, Uno K, Ito M, Minami S, Yanagida H, Taneichi H, Hosono N, Tsuji T, Suzuki T, Sudo H, Kotani T, Yonezawa I, Londono D, Gordon D, Herring JA, Watanabe K, Chiba K, Kamatani N, Jiang Q, Hiraki Y, Kubo M, Toyama Y, Tsunoda T, Wise CA, Qiu Y, Shukunami C, Matsumoto M, Ikegawa S. 2013. Genetic variants in GPR126 are associated with adolescent idiopathic scoliosis. *Nature Genetics* **45**:676–679.

Kou I, Watanabe K, Takahashi Y, Momozawa Y, Khanshour A, Grauers A, Zhou H, Liu G, Fan Y-H, Takeda K, Ogura Y, Zhou T, Iwasaki Y, Kubo M, Wu Z, Matsumoto M, Einarsdottir E, Kere J, Huang D, Qiu G, Qiu Y, Wise CA, Song Y-Q, Wu N, Su P, Gerdhem P, Ikegawa S. 2018. A multi-ethnic meta-analysis confirms the association of rs6570507 with adolescent idiopathic scoliosis. *Scientific Reports* **8**:11575.

Küffer A, Lakkaraju AKK, Mogha A, Petersen SC, Airich K, Doucerain C, Marpakwar R, Bakirci P, Senatore A, Monnard A, Schiavi C, Nuvolone M, Grosshans B, Hornemann S, Bassilana F, Monk KR, Aguzzi A. 2016. The prion protein is an agonistic ligand of the G protein-coupled receptor Adgrg6. *Nature* **536**:464–468.

Leon K, Cunningham RL, Riback JA, Feldman E, Li J, Sosnick TR, Zhao M, Monk KR, Araç D. 2020. Structural basis for adhesion G protein-coupled receptor Gpr126 function. *Nature Communications* **11**:194.

Liebscher I, Schön J, Petersen SC, Fischer L, Auerbach N, Demberg LM, Mogha A, Cöster M, Simon K-U, Rothemund S, Monk KR, Schöneberg T. 2014. A tethered agonist within the ectodomain activates the adhesion G protein-coupled receptors GPR126 and GPR133. *Cell Reports* **9**:2018–2026.

Lin H-H, Chang G-W, Davies JQ, Stacey M, Harris J, Gordon S. 2004. Autocatalytic cleavage of the EMR2 receptor occurs at a conserved G protein-coupled receptor proteolytic site motif. *The Journal of Biological Chemistry* **279**:31823–31832.

Liu G, Liu S, Lin M, Li X, Chen W, Zuo Y, Liu J, Niu Y, Zhao S, Long B, Wu Z, Wu N, Qiu G. 2018. Genetic polymorphisms of GPR126 are functionally associated with PUMC classifications of adolescent idiopathic scoliosis in a Northern Han population. *Journal of Cellular and Molecular Medicine* **22**:1964–1971.

Lou E, Fujisawa S, Morozov A, Barlas A, Romin Y, Dogan Y, Gholami S, Moreira AL, Manova-Todorova K, Moore MAS. 2012. Tunneling nanotubes provide a unique conduit for intercellular transfer of cellular contents in human malignant pleural mesothelioma. *PloS One* **7**:e33093.

Man GC-W, Tang NL-S, Chan TF, Lam TP, Li JW, Ng BK-W, Zhu Z, Qiu Y, Cheng JC-Y. 2019. Replication Study for the Association of GWAS-associated Loci With Adolescent Idiopathic Scoliosis Susceptibility and Curve Progression in a Chinese Population. *Spine* **44**:464–471.

Mierke CT, Kollmannsberger P, Zitterbart DP, Smith J, Fabry B, Goldmann WH. 2008. Mechano-coupling and regulation of contractility by the vinculin tail domain. *Biophysical Journal* **94**:661–670.

Millan MJ, Maiofiss L, Cussac D, Audinot V, Boutin J-A, Newman-Tancredi A. 2002. Differential actions of antiparkinson agents at multiple classes of monoaminergic receptor. I. A multivariate analysis of the binding profiles of 14 drugs at 21 native and cloned human receptor subtypes. *The Journal of Pharmacology and Experimental Therapeutics* **303**:791–804.

Mogha A, Benesh AE, Patra C, Engel FB, Schöneberg T, Liebscher I, Monk KR. 2013. Gpr126 functions in Schwann cells to control differentiation and myelination via G-protein activation. *The Journal of Neuroscience* **33**:17976–17985.

Mogha A, Harty BL, Carlin D, Joseph J, Sanchez NE, Suter U, Piao X, Cavalli V, Monk KR. 2016. Gpr126/Adgrg6 Has Schwann Cell Autonomous and Nonautonomous Functions in Peripheral Nerve Injury and Repair. *The Journal of Neuroscience* **36**:12351–12367.

Monk KR, Naylor SG, Glenn TD, Mercurio S, Perlin JR, Dominguez C, Moens CB, Talbot WS. 2009. A G Protein-Coupled Receptor Is Essential for Schwann Cells to Initiate Myelination. *Science* **325**:1402–1405.

Monk KR, Oshima K, Jors S, Heller S, Talbot WS. 2011. Gpr126 is essential for peripheral nerve development and myelination in mammals. *Development* **138**:2673–2680.

Moriguchi T, Haraguchi K, Ueda N, Okada M, Furuya T, Akiyama T. 2004. DREG, a developmentally regulated G protein-coupled receptor containing two conserved proteolytic cleavage sites. *Genes to Cells* **9**:549–560.

Paavola KJ, Sidik H, Zuchero JB, Eckart M, Talbot WS. 2014. Type IV collagen is an activating ligand for the adhesion G protein-coupled receptor GPR126. *Science Signaling* **7**:ra76.

Petersen SC, Luo R, Liebscher I, Giera S, Jeong S-J, Mogha A, Ghidinelli M, Feltri ML, Schöneberg T, Piao X, Monk KR. 2015. The Adhesion GPCR GPR126 Has Distinct, Domain-Dependent Functions in Schwann Cell Development Mediated by Interaction with Laminin-211. *Neuron* **85**:755–769.

720 **Qin X**, Xu L, Xia C, Zhu W, Sun W, Liu Z, Qiu Y, Zhu Z. 2017. Genetic Variant of GPR126 Gene is
721 Functionally Associated With Adolescent Idiopathic Scoliosis in Chinese Population. *Spine*
722 **42**:E1098-E1103.
723 **Ravenscroft G**, Nolent F, Rajagopalan S, Meireles AM, Paavola KJ, Gaillard D, Alanio E, Buckland
724 M, Arbuckle S, Krivanek M, Maluenda J, Pannell S, Gooding R, Ong RW, Allcock RJ, Carvalho
725 EDF, Carvalho MDF, Kok F, Talbot WS, Melki J, Laing NG. 2015. Mutations of GPR126 are
726 responsible for severe arthrogryposis multiplex congenita. *The American Journal of Human Genetics*
727 **96**:955–961.
728 **Schindelin J**, Arganda-Carreras I, Frise E, Kaynig V, Longair M, Pietzsch T, Preibisch S, Rueden C,
729 Saalfeld S, Schmid B, Tinevez J-Y, White DJ, Hartenstein V, Eliceiri K, Tomancak P, Cardona A.
730 2012. Fiji: an open-source platform for biological-image analysis. *Nature Methods* **9**:676–682.
731 **Scholz N**, Gehring J, Guan C, Ljaschenko D, Fischer R, Lakshmanan V, Kittel RJ, Langenhan T. 2015.
732 The adhesion GPCR latrophilin/CIRL shapes mechanosensation. *Cell Reports* **11**:866–874.
733 **Scholz N**, Guan C, Nieberler M, Grotemeyer A, Maiellaro I, Gao S, Beck S, Pawlak M, Sauer M, Asan
734 E, Rothemund S, Winkler J, Prömel S, Nagel G, Langenhan T, Kittel RJ. 2017. Mechano-dependent
735 signaling by Latrophilin/CIRL quenches cAMP in proprioceptive neurons. *eLife* **6**.
736 **Schöneberg T**, Schulz A, Biebermann H, Grüters A, Grimm T, Hübschmann K, Filler G, Gudermann
737 T, Schultz G. 1998. V2 vasopressin receptor dysfunction in nephrogenic diabetes insipidus caused by
738 different molecular mechanisms. *Human Mutation* **12**:196–205.
739 **Slattery AD**, Blanch AJ, Quinton JS, Gibson CT. 2013. Accurate measurement of Atomic Force
740 Microscope cantilever deflection excluding tip-surface contact with application to force calibration.
741 *Ultramicroscopy* **131**:46–55.
742 **Stoveken HM**, Hajduczok AG, Xu L, Tall GG. 2015. Adhesion G protein-coupled receptors are
743 activated by exposure of a cryptic tethered agonist. *Proceedings of the National Academy of Sciences*
744 *of the United States of America* **112**:6194–6199.
745 **Suchý T**, Zieschang C, Popkova Y, Kaczmarek I, Weiner J, Liebing A-D, Çakir MV, Landgraf K,
746 Gericke M, Pospisilik JA, Körner A, Heiker JT, Dannenberger D, Schiller J, Schöneberg T, Liebscher
747 I, Thor D. 2020. The repertoire of Adhesion G protein-coupled receptors in adipocytes and their
748 functional relevance. *International Journal of Obesity*.
749 **Sun P**, He L, Jia K, Yue Z, Li S, Jin Y, Li Z, Siwko S, Xue F, Su J, Liu M, Luo J. 2020. Regulation of
750 body length and bone mass by Gpr126/Adgrg6. *Science Advances* **6**:eaaz0368.
751 **Takeda K**, Kou I, Hosogane N, Otomo N, Yagi M, Kaneko S, Kono H, Ishikawa M, Takahashi Y,
752 Ikegami T, Nojiri K, Okada E, Funao H, Okuyama K, Tsuji T, Fujita N, Nagoshi N, Tsuji O, Ogura
753 Y, Ishii K, Nakamura M, Matsumoto M, Ikegawa S, Watanabe K. 2019. Association of Susceptibility
754 Genes for Adolescent Idiopathic Scoliosis and Intervertebral Disc Degeneration With Adult Spinal
755 Deformity. *Spine* **44**:1623–1629.

Unal H, Jagannathan R, Karnik SS. 2012. Mechanism of GPCR-directed autoantibodies in diseases. *Advances in Experimental Medicine and Biology* **749**:187–199.

Wilde C, Fischer L, Lede V, Kirchberger J, Rothemund S, Schöneberg T, Liebscher I. 2016. The constitutive activity of the adhesion GPCR GPR114/ADGRG5 is mediated by its tethered agonist. *FASEB Journal* **30**:666–673.

Xu E, Lin T, Jiang H, Ji Z, Shao W, Meng Y, Gao R, Zhou X. 2019a. Asymmetric expression of GPR126 in the convex/concave side of the spine is associated with spinal skeletal malformation in adolescent idiopathic scoliosis population. *European Spine Journal* **28**:1977–1986.

Xu E, Shao W, Jiang H, Lin T, Gao R, Zhou X. 2019b. A Genetic Variant in GPR126 Causing a Decreased Inclusion of Exon 6 Is Associated with Cartilage Development in Adolescent Idiopathic Scoliosis Population. *BioMed Research International* **2019**:4678969.

Xu J-F, Yang G, Pan X-H, Zhang S-J, Zhao C, Qiu B-S, Gu H-F, Hong J-F, Cao L, Chen Y, Xia B, Bi Q, Wang Y-P. 2015. Association of GPR126 gene polymorphism with adolescent idiopathic scoliosis in Chinese populations. *Genomics* **105**:101–107.

Xu L, Wu Z, Xia C, Tang N, Cheng JCY, Qiu Y, Zhu Z. 2019. A Genetic Predictive Model Estimating the Risk of Developing Adolescent Idiopathic Scoliosis. *Current Genomics* **20**:246–251.

Yona S, Lin H-H, Dri P, Davies JQ, Hayhoe RPG, Lewis SM, Heinsbroek SEM, Brown KA, Perretti M, Hamann J, Treacher DF, Gordon S, Stacey M. 2008. Ligation of the adhesion-GPCR EMR2 regulates human neutrophil function. *FASEB Journal* **22**:741–751.